

Engineering of Halide Cation in All-Inorganic Perovskite with Full-Color Luminescence

Cuili Gai¹, Dawei He¹, Yongsheng Wang^{1,*}, Jigang Wang^{2,*}  and Junming Li³

¹ Key Laboratory of Luminescence and Optical Information, Ministry of Education, Institute of Optoelectronic Technology, Beijing Jiao Tong University, Beijing 100044, China; 15118443@bjtu.edu.cn (C.G.); dwhe@bjtu.edu.cn (D.H.)

² Beijing Key Laboratory of Printing and Packaging Materials and Technology, Beijing Institute of Graphic Communication, Beijing 102600, China

³ Beijing Key Laboratory for Sensor, Beijing Information Science and Technology University, Beijing 100085, China; li@physik.hu-berlin.de

* Correspondence: yshwang@bjtu.edu.cn (Y.W.); jigangwang@bigc.edu.cn (J.W.); Tel.: +86 18500863736 (J.W.)

Abstract: All-inorganic halide perovskites are emerging as a class of superstar semiconductors with excellent optoelectronic properties and show great potential for a broad range of applications in solar cells, lighting diodes, X-ray imaging, and photodetectors. Tremendous research about their device performance has been performed since 2015. In this study, we synthesized the all-inorganic perovskite by the hot-injection method and particularly investigated their crystal structural and photoluminescence properties. By halide anion engineering, the all-inorganic perovskites showed a high-symmetry cubic phase. They also showed a tunable optical bandgap, and almost the full color luminescence was achieved (434 to 624 nm). These basic optoelectronic properties could give a guide for further development of this area.

Keywords: perovskite solar cell; thin film; crystal structure; photoluminescence



Citation: Gai, C.; He, D.; Wang, Y.; Wang, J.; Li, J. Engineering of Halide Cation in All-Inorganic Perovskite with Full-Color Luminescence. *Coatings* **2021**, *11*, 330. <https://doi.org/10.3390/coatings11030330>

Academic Editor: Sunil Kumar

Received: 5 February 2021

Accepted: 10 March 2021

Published: 13 March 2021

Publisher's Note: MDPI stays neutral with regard to jurisdictional claims in published maps and institutional affiliations.



Copyright: © 2021 by the authors. Licensee MDPI, Basel, Switzerland. This article is an open access article distributed under the terms and conditions of the Creative Commons Attribution (CC BY) license (<https://creativecommons.org/licenses/by/4.0/>).

1. Introduction

Recently, halide perovskites have been extensively studied due to their fascinating optoelectronic properties, such as tunable bandgaps, high absorption range and coefficients (up to 10^5 cm^{-1}), long minority carrier lifetimes, low-cost fabrication process, flexible device, etc. [1,2]. A wide range of optoelectronic applications have been developed with them as the active layer, e.g., perovskite solar cells (PSCs), perovskite light-emitting diodes (PeLEDs), perovskite photodetectors, and perovskite sensors. For instance, Miyasaka et al. first discovered PSCs in 2009 [3], and the power conversion efficiency (PCE) has nowadays rapidly boosted to 25.5%, already surpassing that of commercial silicon solar cells [4]. Dan et al. reported perovskite organic light-emitting diodes (PeOLEDs) in 2014 for the first time [5], and the maximum external quantum efficiency (EQE) has today increased to over 20%, which is comparable to that of conventional OLEDs or quantum dot light-emitting diodes (QLEDs) [6]. In general, halide perovskites have a chemical formula of ABX_3 , where A represent a large monovalent cation, such as organic methylammonium (MA: CH_3NH_3) and inorganic cesium (Cs). B is a bivalent metal cation, such as Pb and Sn. The X anion, as the name implies, is a halogen anion: Cl, Br, I, and mixed Cl/Br/I systems. With the inorganic Cs cation at A position, CsPbX_3 perovskite shows a significantly improve stability, which has already proven in the solid-state dye sensitized solar cells and previous PSC study [7,8].

One of the most fascinating properties of CsPbX_3 perovskite materials is their tunable bandgaps, which have allowed them to achieve astonishing breakthrough in a variety of optoelectronic applications. For instance, the ideal bandgap for PSCs is 1.34 eV [9–11]; the ideal bandgap for tandem photovoltaic devices (top sub-cell) is 1.70 eV [12]; and the ideal bandgaps for PeLED are 1.80, 2.30, and 2.70 eV for red, green, and blue emission,

respectively. It has been proposed that in the CsPbX₃ system, the Cs cation acts to fulfill charge neutrality within the lattice and only slightly affects the electronic states [13]. The valance band of CsPbX₃ is predominately formed by mixing the halide np^6 orbitals (n is the principal quantum number, Cl: $n = 3$, Br: $n = 4$, and I: $n = 5$) and ns^2 orbitals from the lead ($n = 5$), while the conduction band mainly arises from antibonding mixing of the lead and the halide np^6 orbital; thus, the X cation plays the main role in the determination of the bandgap [14,15]. Therefore, with the mixed halogen cation, a wide broad bandgap CsPbX₃ could be achieved. Although the CsPbX₃ perovskites were reported as early as 1958 [16], investigation of their application in optoelectronic devices had not been conducted until 2015 [17,18]. After that, there has been tremendous research on optoelectronic device performance. Noh et al. demonstrated excellent perovskite solar cells based on organic–inorganic perovskite MAPbI_{3–x}Br_x [17]. Guhrenz et al. demonstrated an excellent light-emitting device based on a mix of CsPbCl₃, CsPbBr₃, and CsPbI₃ [18]. Motivated by this, in this study, we systematically varied the halogen anion and synthesized CsPbCl₃, CsPbCl_{2.5}Br_{0.5}, CsPbCl₂Br, CsPbCl_{1.5}Br_{1.5}, CsPbClBr₂, CsPbCl_{0.5}Br_{2.5}, CsPbBr₃, CsPbBr_{2.5}I_{0.5}, CsPbBr₂I, CsPbBr_{1.5}I_{1.5}, CsPbBrI₂, CsPbBr_{0.5}I_{2.5}, and CsPbI₃ by the hot-injection method, and their crystal structural and photoluminescence properties were systematically studied.

2. Materials and Methods

Preparation of Cs-oleate: Oleic acid (OA, 90%), oleylamine (OAm, 90%), octadecene (ODE, 99%), Cs₂CO₃ (98%), lead iodide (99%), cesium bromide (>98%), cesium chloride (98%), and cesium iodide (99%) were purchased from Sigma-Aldrich (Shanghai, China). Cs₂CO₃ (0.4 g, 1.23 mmol), 15 mL ODE, and 1.25 mL OA were loaded into a 50 mL three-necked flask and dried for 0.5 h at 100 °C with stirring and then heated under N₂ to 150 °C until all Cs₂CO₃ reacted with OA (transparent solution). Because Cs-oleate precipitated out of ODE at below 100 °C, it had to be annealed to 150 °C before CsPbX₃ perovskite synthesis.

Synthesis of CsPbX₃: All-inorganic perovskites were synthesized by a hot-injection method according to Protesescu's work [17]. In this study, 0.36 mmol PbX₂ (X = Cl, Br, and I), OAm (1.0 mL), oleylamine (1.0 mL), and octadecene (10 mL) were added to a three-necked round-bottom flask (25 mL). The resulting mixture was heated to 100 °C with stirring and maintained for 0.5 h. At this time, the water residue was removed by nitrogen purging and vacuum aspiration, and the mixture was heated to 160 °C until the PbX₂ precursor was completely dissolved. Then, the hot cesium oleate precursor solution (1 mL) was quickly injected into the above reaction mixture. After 5 s reaction, the flask was quickly transferred to the ice bath, and the obtained CsPbX₃ was kept by centrifugation at 10,000 rpm for 10 min and stored in cyclohexane (4 mL) before further use.

Synthesis of CsPbX₃ (X = Cl, Br, or I) nanocrystals containing mixed halogens: a mmol of PbX₂ (X = Cl, Br, or I) and (0.36 – a) mmol of another PbX₂ (X = Cl, Br, or I), OA (1.0 mL), OAm (1.0 mL), and ODE (10 mL) were added to a three-necked round-bottom flask (50 mL). Then, it was annealed to 100 °C with stirring and maintained for 30 min. Then, it was heated to 160 °C until the PbX₂ precursor was completely dissolved. The hot cesium OA solution (1 mL) was quickly injected into the above solution, and after 5 s reaction, the flask was quickly transferred to the ice bath. The obtained CsPbX₃ perovskite was kept by centrifugation at 10,000 rpm for 5 min and stored in cyclohexane prior to further use. The added amount were as follows: CsPbCl₃ (PbCl₂: 100.12 mg), CsPbCl_{2.5}Br_{0.5} (PbCl₂: 83.43 mg, PbBr₂: 22.02 mg), CsPbCl₂Br (PbCl₂: 66.72 mg, PbBr₂: 44.04 mg), CsPbCl_{1.5}Br_{1.5} (PbCl₂: 50.06 mg, PbBr₂: 66.06 mg), CsPbClBr₂ (PbCl₂: 33.37 mg, PbBr₂: 88.08 mg), CsPbCl_{0.5}Br_{2.5} (PbCl₂: 16.69 mg, PbBr₂: 132.03 mg), CsPbBr₃ (PbBr₂: 132.12 mg), CsPbBr_{2.5}I_{0.5} (PbBr₂: 110.01 mg, PbI₂: 27.66 mg), CsPbBr₂I (PbBr₂: 88.08 mg, PbI₂: 55.32 mg), CsPbBr_{1.5}I_{1.5} (PbBr₂: 66.06 mg, PbI₂: 82.99 mg), CsPbBrI₂ (PbBr₂: 43.67 mg, PbI₂: 110.64 mg), CsPbBr_{0.5}I_{2.5} (PbBr₂: 22.02 mg, PbI₂: 138.30 mg), and CsPbI₃ (PbI₂: 165.96 mg).

X-ray diffraction (XRD) pattern characterization: The experiment was performed by XRD diffraction device (Bruker D8 Advanced diffractometer with Cu K α radiation, Bruker,

Billerica, MA, USA). First, 100 μL of the sample was taken onto the slide and dried under nitrogen atmosphere to make cyclohexane volatilize, which was then tested and analyzed.

Photoluminescence characterization: The experiment was carried out using a fluorescence spectrometer model Fluorolog-3. First, 100 μL of the sample was taken and added to a quartz cuvette. Then, 4 mL of cyclohexane was added, and the luminescence wavelengths under 365 nm excitation were tested and analyzed.

3. Results

We began by studying how the X cation influenced the optoelectronic properties based on CsPbX_3 with monohalogen (Cl, Br, and I). Figure 1a exhibits their XRD patterns monitored in the 2θ range of 10° to 45° , which matched well with the literature. With hot-injection preparation methods, the halogen cation engineering did not change the crystal structure. All CsPbX_3 showed a high-symmetry cubic phase with the space group $pm\bar{3}m$ due to the high reaction temperature in the preparation process and also the contribution from the surface energy of the nanocrystal [17,19,20]. CsPbCl_3 showed three dominant diffraction peaks: (100) at $2\theta = 15.5^\circ$, (110) at $2\theta = 22.1^\circ$, and (200) at $2\theta = 31.3^\circ$ (ID: mp-23037). CsPbBr_3 also showed three dominant diffraction peaks: (100) at $2\theta = 14.8^\circ$, (110) at $2\theta = 20.9^\circ$, and (200) at $2\theta = 29.7^\circ$ (ID: mp-600089). CsPbI_3 showed more diffraction peaks than those of the above two: (100) at $2\theta = 13.9^\circ$, (110) at $2\theta = 19.6^\circ$, (200) at $2\theta = 27.9^\circ$, (210) at $2\theta = 31.2^\circ$, (211) at 33.9° , (220) at 40.2° , and (300) at 42.3° (ID: mp-1069538). The optical properties of these CsPbX_3 were studied by stable photoluminescence, as shown in Figure 1b. We found that an increase in the cation size resulted in a reduction in the optical bandgap, which was 2.90 eV for CsPbCl_3 , 2.40 eV for CsPbBr_3 , and 2.00 eV for CsPbI_3 . The difference in optical properties originated from the difference in the ionic radius of halide ions with six-fold coordination, which was 1.81, 1.96, and 2.20 \AA for Cl^- , Br^- , and I^- , respectively. The CsPbCl_3 perovskite exhibited the PL peak at 434 nm with full width at half maximum (FWHM) = 16 nm (blue color emission); the CsPbBr_3 perovskite showed PL peak at 507 nm and FWHM = 23 nm (green color emission); and the CsPbI_3 perovskite showed PL peak at 625 nm with FWHM = 37 nm (red color emission).

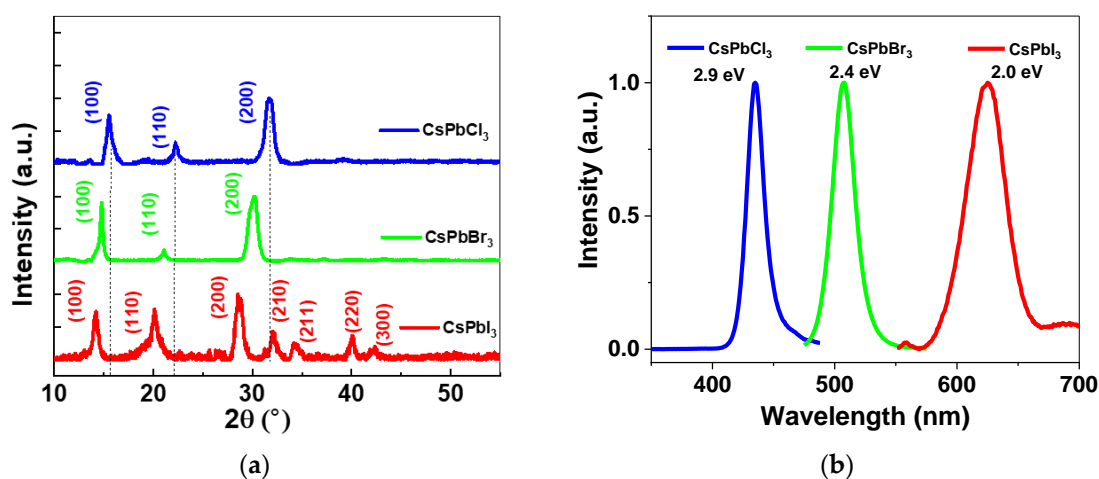


Figure 1. (a) X-ray diffraction patterns from CsPbX_3 perovskite synthesized by hot-injection methods. (b) Photoluminescence emission spectra of CsPbX_3 perovskite. Note that their main diffraction peaks and optical bandgaps are shown in inset of (a) and (b), respectively.

We then studied the influence of mixed halogen cation based on $\text{CsPbCl}_y\text{Br}_{3-y}$ ($y = 0, 0.5, 1, 1.5, 2, 2.5, \text{ and } 3$). From the XRD patterns (Figure 2a), the diffraction peaks exhibited successive shift, which was linearly dependent on the halide composition. The composition modulation of halide anions does not affect the cationic sublattice; meanwhile, the cubic structure is still maintained [21]. Moreover, it means the precursor solutions should be uniform during the film fabrication procedure. From the PL spectra shown in Figure 2b,

we also found the successively red shift emission peaks, which were 434 nm for CsPbCl₃, 446 nm for CsPbCl_{2.5}Br_{0.5}, 453 nm for CsPbCl₂Br, 471 nm for CsPbCl_{1.5}Br_{1.5}, 490 nm for CsPbClBr₂, 499 nm for CsPbCl_{0.5}Br_{2.5}, and 507 nm for CsPbBr₃ perovskites, respectively. The redshift of the PL peaks indicated that the Cl anion was gradually replaced by Br to form CsPbCl_yBr_{3-y} ($y = 0, 0.5, 1, 1.5, 2, 2.5, \text{ and } 3$).

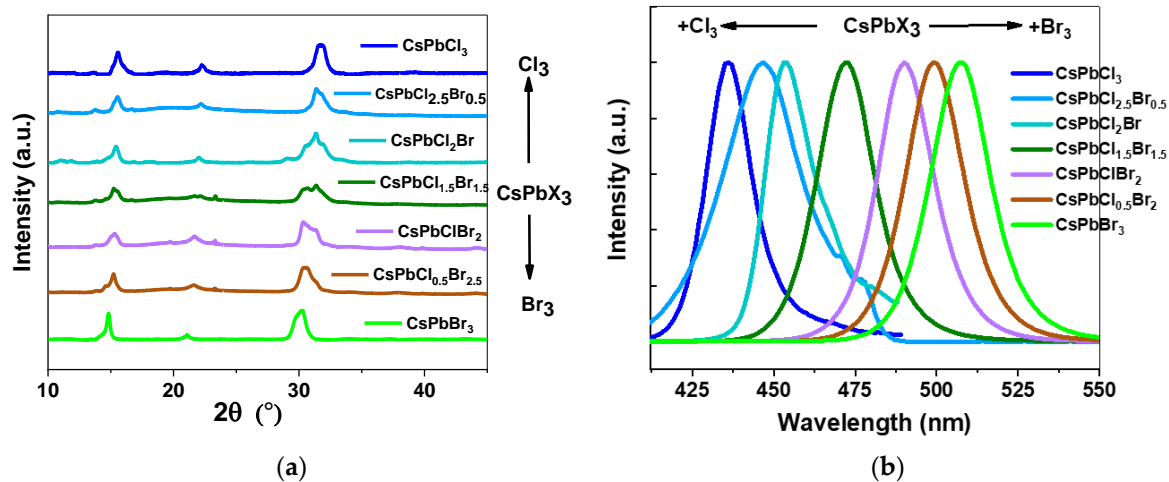


Figure 2. (a) X-ray diffraction patterns and (b) photoluminescence spectra for mixed-halide CsPbCl_yBr_{3-y} ($y = 0, 0.5, 1, 1.5, 2, 2.5, \text{ and } 3$)

We further studied the influence of mixed halogen cation based on CsPbBr_yI_{3-y} ($y = 0, 0.5, 1, 1.5, 2, 2.5, \text{ and } 3$). They exhibited similar trends as observed in CsPb(Cl/Br)₃ perovskites (as shown in Figure 3). The XRD peaks showed a successive shift, which was linearly dependent on the composition. The successive redshift of the photoluminescence peak was also observed, indicating that the Br anion was gradually mixed with I anion and formed CsPbBr_yI_{3-y} ($y = 0, 0.5, 1, 1.5, 2, 2.5, \text{ and } 3$) perovskite.

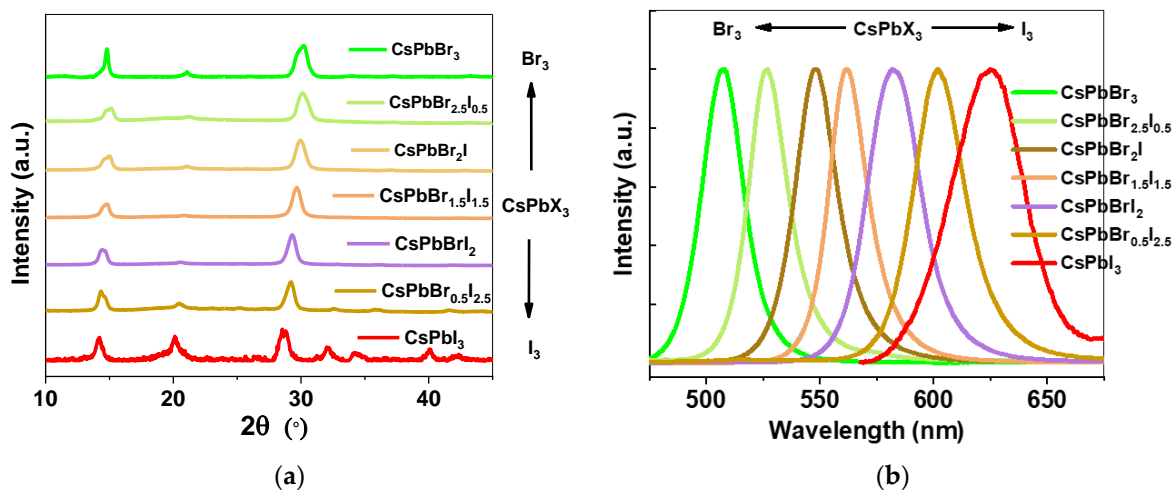


Figure 3. (a) X-ray diffraction patterns and (b) photoluminescence spectra for mixed-halide CsPbBr_yI_{3-y} ($y = 0, 0.5, 1, 1.5, 2, 2.5, \text{ and } 3$).

4. Conclusions

In summary, we synthesized and characterized CsPbX₃ by adjusting the halogen anions (Cl, Br, I, mixed Cl/Br, and mixed Br/I). With controllable hot-injection methods, these all-inorganic perovskites exhibited a high-symmetry cubic phase. Meanwhile, by halogen anion engineering, they showed a successive tunable optical bandgap with luminescence covering the entire visible range (434–625 nm). Moreover, the successive bandgap

energy of CsPbX₃ were found to have a linear relationship with the halogen content. We are convinced that the present findings will be helpful for the development of promising related application, such as all-inorganic perovskite solar cells, perovskite light-emitting diodes, and perovskite photodetectors.

Author Contributions: Investigation: C.G. and J.W.; funding acquisition: Y.W. and J.W.; writing—original draft preparation: D.H. and J.L. All authors have read and agreed to the published version of the manuscript.

Funding: This research was funded by the National Natural Science Foundation of China (Grant Nos. 52002074, 2016YFA0202302, 61527817, 61845236, 52002074, 51602071, and 11427808), Beijing Social Science Foundation (No. 15LSC014), Beijing Natural Science Foundation (4132031), Beijing Postdoctoral Research Foundation, Beijing University Student Research Program, Beijing City College High-level Teachers Team Construction Program for the Young Top Talents Training (CIT&TCD201904050), and the Open Research Subject of Key Laboratory of Dielectric and Electrolyte Functional Material Hebei Province (No. HKDE201902).

Institutional Review Board Statement: Not applicable.

Informed Consent Statement: Not applicable.

Data Availability Statement: The data used to support the findings of this study are available from the corresponding author upon request.

Conflicts of Interest: The authors declare no conflict of interest.

References

1. Abdi-Jalebi, M.; Andaji-Garmaroudi, Z.; Cacovich, S.; Stavrakas, C.; Philippe, B.; Richter, J.M.; Alsari, M.; Booker, E.P.; Hutter, E.M.; Pearson, A.J.; et al. Maximizing and stabilizing luminescence from halide perovskites with potassium passivation. *Nature* **2018**, *555*, 497–501. [[CrossRef](#)] [[PubMed](#)]
2. Kim, G.; Min, H.; Lee, K.S.; Lee, D.Y.; Yoon, S.M.; Seok, S.I. Impact of strain relaxation on performance of α -formamidinium lead iodide perovskite solar cells. *Science* **2020**, *370*, 108–112. [[CrossRef](#)] [[PubMed](#)]
3. Kojima, A.; Teshima, K.; Shirai, Y.; Miyasaka, T. Organometal halide perovskites as visible-light sensitizers for photovoltaic cells. *J. Am. Chem. Soc.* **2009**, *131*, 6050–6051. [[CrossRef](#)] [[PubMed](#)]
4. Chart, Best Research-Cell Efficiency Chart. Available online: <https://www.nrel.gov/pv/cell-efficiency.html> (accessed on 20 December 2020).
5. Tan, Z.-K.; Moghaddam, R.S.; Lai, M.L.; Docampo, P.; Higler, R.; Deschler, F.; Price, M.; Sadhanala, A.; Pazos, L.M.; Credgington, D. Bright light-emitting diodes based on organometal halide perovskite. *Nat. Nanotechnol.* **2014**, *9*, 687–692. [[CrossRef](#)] [[PubMed](#)]
6. Kim, Y.-H.; Kim, S.; Kakekhani, A.; Park, J.; Park, J.; Lee, Y.-H.; Xu, H.; Nagane, S.; Wexler, R.B.; Kim, D.-H.; et al. Comprehensive defect suppression in perovskite nanocrystals for high-efficiency light-emitting diodes. *Nat. Photonics* **2021**, *15*, 148–155. [[CrossRef](#)]
7. Lee, B.; He, J.; Chang, R.P.; Kanatzidis, M.G. All-solid-state dye-sensitized solar cells with high efficiency. *Nature* **2012**, *485*, 486.
8. Li, J.; Huang, J.; Zhao, A.; Li, Y.; Wei, M. An inorganic stable Sn-based perovskite film with regulated nucleation for solar cell application. *J. Mater. Chem. C* **2020**, *8*, 8840–8845. [[CrossRef](#)]
9. Shockley, W.; Queisser, H.J. Detailed balance limit of efficiency of p-n junction solar cells. *J. Appl. Phys.* **1961**, *32*, 510–519. [[CrossRef](#)]
10. Rühle, S. Tabulated values of the Shockley–Queisser limit for single junction solar cells. *J. Sol. Energy* **2016**, *130*, 139–147. [[CrossRef](#)]
11. Li, J.; Hu, P.; Chen, Y.; Li, Y.; Wei, M. Enhanced performance of Sn-based perovskite solar cells by two-dimensional perovskite doping. *ACS Sustain. Chem. Eng.* **2020**, *8*, 8624–8628. [[CrossRef](#)]
12. Zhao, D.; Ding, L. All-perovskite tandem structures shed light on thin-film photovoltaics. *Sci. Bull.* **2020**, *65*, 1144–1146. [[CrossRef](#)]
13. Borriello, I.; Cantele, G.; Ninno, D. Ab initio investigation of hybrid organic-inorganic perovskites based on tin halides. *Phys. Rev. B* **2008**, *77*, 235214. [[CrossRef](#)]
14. Noh, J.H.; Im, S.H.; Heo, J.H.; Mandal, T.N.; Seok, S.I. Chemical management for colorful, efficient, and stable inorganic-organic hybrid nanostructured solar cells. *Nano Lett.* **2013**, *13*, 1764–1769. [[CrossRef](#)] [[PubMed](#)]
15. Liashenko, T.G.; Cherotchenko, E.D.; Pushkarev, A.P.; Pakštas, V.; Naujokaitis, A.; Khubezhov, S.A.; Polozkov, R.G.; Agapev, K.B.; Zakhidov, A.A.; Shelykh, I.A.; et al. Electronic structure of CsPbBr_{3-x}Cl_x perovskites: Synthesis, experimental characterization, and DFT simulations. *PCCP* **2019**, *21*, 18930–18938. [[CrossRef](#)] [[PubMed](#)]
16. Møller, C.K. Crystal structure and photoconductivity of caesium plumbahalides. *Nature* **1958**, *182*, 1436. [[CrossRef](#)]
17. Protesescu, L.; Yakunin, S.; Bodnarchuk, M.I.; Krieg, F.; Caputo, R.; Hendon, C.H.; Yang, R.X.; Walsh, A.; Kovalenko, M.V. Nanocrystals of cesium lead halide perovskites (CsPbX₃, X = Cl, Br, and I): Novel optoelectronic materials showing bright emission with wide color gamut. *Nano Lett.* **2015**, *15*, 3692–3696. [[CrossRef](#)] [[PubMed](#)]

18. Guhrenz, C.; Benad, A.; Ziegler, C.; Haubold, D.; Gaponik, N.; Eychmüller, A. Solid-state anion exchange reactions for color tuning of CsPbX₃ perovskite nanocrystals. *Chem. Mater.* **2016**, *28*, 9033–9040. [[CrossRef](#)]
19. Harada, J.; Sakata, M.; Hoshino, S.; Hirotsu, S. Neutron diffraction study of the structure in cubic CsPbCl₃. *J. Phys. Soc. Jpn.* **1976**, *40*, 212–218. [[CrossRef](#)]
20. Sutton, R.J.; Filip, M.R.; Haghighirad, A.A.; Sakai, N.; Wenger, B.; Giustino, F.; Snaith, H.J. Cubic or orthorhombic? Revealing the crystal structure of metastable black-phase CsPbI₃ by theory and experiment. *ACS Energy Lett.* **2018**, *3*, 1787–1794. [[CrossRef](#)]
21. Nedelcu, G.; Protesescu, L.; Yakunin, S.; Bodnarchuk, M.I.; Grotevent, M.J.; Kovalenko, M.V. Fast anion-exchange in highly luminescent nanocrystals of cesium lead halide perovskites (CsPbX₃, X= Cl, Br, I). *Nano Lett.* **2015**, *15*, 5635–5640. [[CrossRef](#)] [[PubMed](#)]